An atomic resolution view of ICAM recognition in a complex between the binding domains of ICAM-3 and integrin $\alpha_L\beta_2$

Gang Song*†, Yuting Yang†‡§, Jin-huan Liu‡, Jose M. Casasnovas*¶, Motomu Shimaoka*, Timothy A. Springer*‖, and Jia-huai Wang‡‖

*CBR Institute for Biomedical Research, Department of Pathology, Harvard Medical School, Boston, MA 02115; and ‡Dana–Farber Cancer Institute, Department of Pediatrics, and Department of Biological Chemistry and Molecular Pharmacology, Harvard Medical School, Boston, MA 02115

Contributed by Timothy A. Springer, January 4, 2005

Within the Ig superfamily (IgSF), intercellular adhesion molecules (ICAMs) form a subfamily that binds the leukocyte integrin $\alpha_L\beta_2$. We report a 1.65-Å-resolution crystal structure of the ICAM-3 N-terminal domain (D1) in complex with the inserted domain, the ligand-binding domain of $\alpha_L\beta_2$. This high-resolution structure and comparisons among ICAM subfamily members establish that the binding of ICAM-3 D1 onto the inserted domain represents a common docking mode for ICAM subfamily members. The markedly different off-rates of ICAM-1, -2, and -3 appear to be determined by the hydrophobicity of residues that surround a metal coordination bond in the $\alpha_L\beta_2$-binding interfaces. Variation in composition of glycans on the periphery of the interfaces influences on-rate.

structure | protein recognition | cell adhesion | LFA-1

ICAMs are type I transmembrane glycoproteins that form a subset of the IgSF. ICAM-1, -2, and -3 function in the immune system, mediating cell adhesion through interaction with the leukocyte integrin $\alpha_L\beta_2$ in different cellular settings. Like other integrins, $\alpha_L\beta_2$ is a large heterodimeric transmembrane protein that functions as a bidirectional and allosteric signaling molecule. The interaction of $\alpha_L\beta_2$ with ICAMs is critical in immune surveillance and responsiveness of leukocytes.

It is intriguing to have three homologous immune receptors, ICAM-1, -2, and –3, that bind to the same integrin. Monoclonal antibodies to all three ICAMs are required to inhibit peripheral blood lymphocyte proliferation in immune responses at the same level as monoclonal antibodies to $\alpha_L\beta_2$, suggesting that multiple $\alpha_L\beta_2$ ligands are required for different aspects of $\alpha_L\beta_2$-dependent leukocyte functions (1). ICAM-1 is thought to be important in leukocyte emigration through the endothelium into sites of immunological challenge (2, 3). ICAM-1 also plays a critical role in forming the immunological synapse between lymphocytes and their target cells, by promoting cell adhesion and lowering the activation threshold. In the absence of ICAM-1/$\alpha_L\beta_2$ interaction, 100-fold more antigen is required for T cell activation (4). ICAM-2 is the predominant ligand for $\alpha_L\beta_2$ on resting endothelial cells and has been suggested to be vital for normal recirculation of resting leukocytes (5). By contrast, ICAM-3 is the major $\alpha_L\beta_2$ ligand on resting T cells, on which ICAM-1 and -2 are either expressed at a very low level or not at all. The ICAM-3/$\alpha_L\beta_2$ adhesive event may facilitate interaction of resting T cells with antigen-presenting B cells as an initial step of immune response (6–8). Moreover, ICAM-3 is a costimulatory molecule for both resting and activated T cells (9). Recent work has provided direct evidence that ICAM-3 is the primary adhesion molecule involved in antigen-independent conjugate formation between T cells and antigen-presenting cells (APCs). This initial contact of a T cell with the APC creates an opportunity for T cells to exert exploratory scanning of the APC surface for antigen recognition (10). The low-affinity ICAM-3/$\alpha_L\beta_2$ interaction also regulates ICAM-1/$\alpha_L\beta_2$-mediated adhesion by augmenting accumulation of $\alpha_L\beta_2$ at sites of adhesion contact (11). Biophysical studies revealed the order in $\alpha_L\beta_2$-binding affinity to be ICAM-1 > ICAM-2 > ICAM-3 (12). An unresolved issue has been what determines these ICAMs' differential $\alpha_L\beta_2$-binding capacities.

Much has been learned over the last few years about the structural features of ICAM-1 and -2 (reviewed in ref. 13) as well as their dynamic binding partner, the inserted (I) domain of $\alpha_L\beta_2$ (reviewed in ref. 14). The I domain bears a Mg^{2+} in its metal-ion-dependent adhesion site (MIDAS) (15), which coordinates with a Glu residue in ICAM-1 at the center of its ligand-binding site (16). Studies on I domains demonstrate three distinct conformations termed closed, intermediate, and open, with low, intermediate, and high affinity for ligand, respectively (16). In intact integrins, conformational signals are transmitted from inside activated lymphocytes that alter the conformation of the I domain and increase its affinity for ligand. Disulfide bonds have been engineered to mimic conformational signals that stabilize integrins in the intermediate and open conformations (16). The previous ICAM-1 complex with the α_L I domain was determined at a 3.3-Å resolution (16). Here, we present a 1.65-Å-resolution structure of ICAM-3 D1 in complex with a high-affinity engineered α_L I domain. The current high-resolution structure allows us to draw the conclusion that ICAM members share an identical docking mechanism onto the α_L I domain and to suggest that hydrophobic interactions within the interface are important in affinity differences among ICAMs. We also demonstrate that deglycosylation of ICAM-3 leads to increased affinity, which provides further insights into the role glycans play on cell surface receptors involved in the immune system.

Methods

Protein Expression, Purification, and Crystallization. The high-affinity, K287C/K294C mutant α_L I domain (G128 to E301) was expressed and purified as described in ref. 12. A cDNA encoding the ICAM-3 signal peptide sequence and residues Q1 to Y86 was subcloned into pBJ5-GS expression vector. Stable Chinese hamster ovary (CHO) Lec3.2.8.1 cells expressing ICAM-3 were established similarly as described in ref. 17. ICAM-3 D1 was

Abbreviations: CHO, Chinese hamster ovary; I domain, inserted domain; MIDAS, metal-ion-dependent adhesion site; SPR, surface plasmon resonance.

Data deposition: The atomic coordinates and structures factors have been deposited in the Protein Data Bank, www.pdb.org (PDB ID code 1T0P).

†G.S. and Y.Y. contributed equally to this work.

§Present address: Rosenstiel Center, Brandeis University, Waltham, MA 02454.

¶Present address: Centro Nacional de Biotecnologia, Consejo Superior de Investigaciones Cientificas, 28049 Madrid, Spain.

‖To whom correspondence may be addressed. E-mail: springer@cbr.med.harvard.edu or jwang@red.dfci.harvard.edu.

Table 1. Crystallographic and refinement statistics

Space group	$P2_12_12_1$
Unit cell (*a*, *b*, *c*), Å	42.5, 66.5, 110.8
Resolution, Å	1.65
Reflections (overall/unique)	220,005/35,921
R_{sym}, % (overall/last shell)	7.9 (52.2)
I/σ (overall/last shell)	28.5/2.4
Completeness, % (overall/last shell)	94.7 (92.3)
Refinement range, Å	30–1.65
Data cutoff ($\|F_o\|$)	0.0
Number of reflections (work/test)	32,291/3,578
R/R_{free}	0.221/0.243
Ramachandran statistics (good/additional/generous/forbidden)	88.5/10.2/0.9/0.4*
rmsd bond lengths, Å/bond angles, °	0.005/1.24
Protein atom average *B* value, Å^2	23.1
Wilson *B* value, Å^2	19.5

*Density of the outlier α_L S174 is very clear.

purified with a mAb (CBR-ICAM3/1) affinity column. Pooled fractions were dialyzed against 20 mM Tris·HCl (pH 7.5)/0.15M NaCl and then treated with 4,000 units of Endo H_f (New England Biolabs) per mg of protein at room temperature overnight. ICAM-3 D1 was further purified by a mono Q column (20 mM Tris·HCl, pH 8.0, eluted with a NaCl gradient).

Crystals were grown by using the vapor-diffusion method in hanging drops at room temperature. ICAM-3 D1 (6 mg/ml in 10 mM Tris·HCl, pH 8.0) and high-affinity I domain (17 mg/ml in 10 mM Tris·HCl, pH 8.0/1 mM $MgCl_2$) were mixed in a 1:1 molar ratio. Equal volumes of protein solution and the reservoir solution of 30% (wt/vol) polyethylene glycol monomethyl ether 5000, 0.2 M $(NH_4)_2SO_4$, and 0.1 M sodium cacodylate (pH 6.4) were then mixed. For data collection, crystals were transferred to a cryo-protectant buffer containing reservoir solution supplemented with 15% (vol/vol) glycerol and flash-frozen in liquid nitrogen.

Structure Determination and Refinements. Data were collected at beamline 19-ID in the Advanced Photon Source of the Argonne National Laboratory and processed with HKL-2000 (18). The structure was determined by using molecular replacement implemented in AMORE (19) based on a two-body search in the 15- to 3.5-Å range. The high-affinity I domain of $\alpha_L\beta_2$ (PDB ID code 1MQA) and domain 1 of ICAM-2 (PDB ID code 1ZXQ) were used as search models. Rigid-body refinement yielded a clean map in which main-chain and side-chain densities were easily seen for model rebuilding of ICAM-3 D1 with O (20). The model was refined to a 1.65-Å resolution by using simulated annealing in CNS 1.1 (21).

Surface Plasmon Resonance (SPR) Measurements. A high-affinity α_L I domain mutant (K287C/K294C, G128 to E301) with a BirA recognition peptide (LGGIFEAMKMELRD) tag fused to the N terminus was constructed for SPR measurements (22, 23). The mutant I domain was expressed in *Escherichia Coli* BL21 DE3 (Novagen), refolded, and purified as described in ref. 12, except that redox buffer (2.5 mM cystamine/5 mM cysteamine) was used during refolding. The I domain was biotinylated with the BirA enzyme (Avidity, Denver) and subjected to Superdex S-200 chromatography in TBS buffer to remove biotin.

SPR experiments were carried out on a Biacore 3000 instrument (Biacore, Piscataway, NJ) at room temperature. Soluble ICAM-1-Fc (R & D Systems) was immobilized on a CM-5 sensor chip by the amine coupling method. A control surface was prepared by *N*-ethyl-*N*′-(3-dimethylaminopropyl)-carbodiimide hydrochloride/*N*-hydroxysuccinimide activation and blocked with ethanolamine. To directly measure the affinity and kinetics between ICAM-3 D1 and the α_L I domain, biotin-labeled high-affinity I domain mutant (K287C/K294C), or biotin as control, was directly captured on an SA sensor chip (Biacore). To perform the inhibition assay, Endo H_f-treated or untreated ICAM-3 D1 was mixed with the high-affinity α_L I domain (50 nM) at room temperature for 15 min and then injected over the sensor chip in 20 mM Tris (pH 8.0)/0.15M NaCl/1 mM Mg^{2+} at 10 μl/min (12).

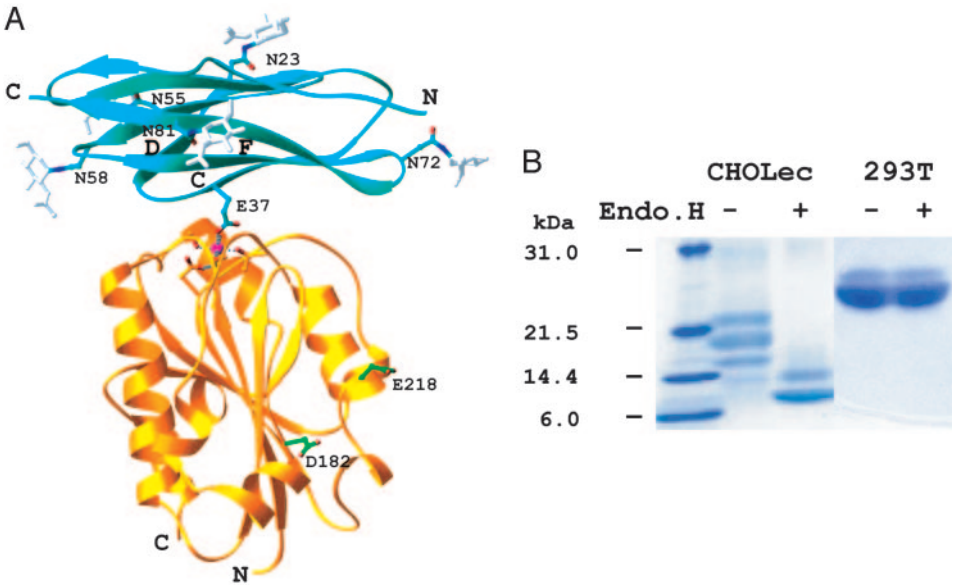

Fig. 1. Overall structure and SDS/PAGE. (*A*) Ribbon diagram of the α_L I domain in complex with domain 1 of ICAM-3. I domain is in gold, and ICAM-3 D1 is in cyan. The Mg^{2+} ion is shown as a magenta sphere. I domain MIDAS and ICAM-3 Glu-37 side chains are shown as a ball-and-stick model. The interacting β strands C, D, and F of ICAM-1 are labeled. Five glycans and their linked asparagines are shown in silver and cyan, respectively. Residues in the epitope of MEM-83, Asp-182 and Glu-218 (42), are highlighted in green. The figure was prepared with RIBBONS (43). (*B*) SDS/PAGE (4–20%) and Coomassie blue staining of ICAM-3 D1 before and after Endo H_f treatment. Positions of molecular weight standards are shown on the left in kDa.

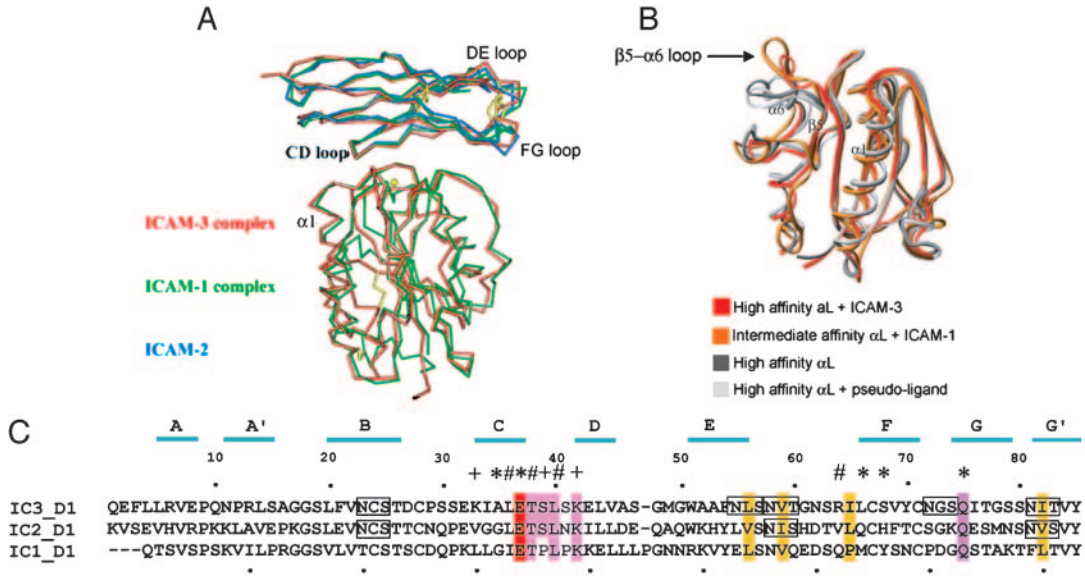

Fig. 2. Structural comparisons among ICAM subfamily members and different mutant α_L I domain crystal forms. (*A*) Superposition of the ICAM-1/α_L I domain complex (PDB code 1MQ8, green) on ICAM-3/α_L I domain complex (red). Only D1s are used for superposition, with all Cα atoms within 2 Å. Also included is the structure of ICAM-2 (PDB ID code 1ZXQ; blue). Domain 2 of ICAM-1 and -2 are omitted for clarity. Note that the CD loops of the three ICAM subfamily members have a remarkably similar conformation. (*B*) Superposition of the pseudoliganded high-affinity I domain (PDB ID code 1MQ9; silver), the unliganded high-affinity I domain (PDB ID code 1MQA; gray), the ICAM-1-liganded intermediate-affinity I domain (PDB ID code 1MQ8; orange), and the ICAM-3-liganded high-affinity α_L I domain (red). *B* is rotated about 60° around the vertical axis from *A*. Notice the significant movement of the β5–α6 loop upon ligation. (*C*) Structure-based sequence alignment of ICAM subfamily members. The alignment is based on three-dimensional structure. The secondary structure elements of ICAM-3 D1 are marked above the sequence. The contact residues are marked (*, side chain interaction; #, backbone H-bonds; +, both side chain and backbone interactions). The critical MIDAS coordinating residue, Glu-37, is colored red. The conserved contact residues in ICAMs and the conserved residues important for restraining the unique conformation of the CD loop are colored magenta and yellow, respectively. The glycosylation sites in ICAM-2 and -3 are boxed. *A* was prepared with SETOR (44), and *B* was prepared with RIBBONS (43).

Results and Discussion

Overall Structure. The crystal structure of ICAM-3 D1 in complex with an α_L I domain mutationally constrained in a high-affinity conformation with a disulfide bond (referred to as ICAM-3/α_L I domain hereafter) was determined to a 1.65-Å resolution by using molecular replacement. Statistics for data collection and structure determination are summarized in Table 1. Fig. 1*A* is a ribbon drawing of the complex structure. Glycans are found N-linked to ICAM-3 residues Asn-23, Asn-55, Asn-58, Asn-72, and Asn-81 (Figs. 1*A* and 2*C*). These carbohydrates are on the periphery of the binding site for the α_L I domain, and on the face of ICAM-3 opposite the binding site. The ABED β-sheet face of D1 that mediates dimerization in ICAM-1 is occluded by the Asn-23 and Asn-72 N-linked glycans in ICAM-3, preventing analogous dimerization of ICAM-3. Lack of dimerization at this interface may affect the manner in which ICAM-3 molecules cluster on the cell surface.

ICAM-3 D1 docks with its CD loop and GFC β-sheet onto a shallow groove on the I domain bearing the MIDAS (Fig. 1*A*). The β strands in ICAM-3 D1 run in a direction approximately perpendicular to the central β-sheet of the I domain. The major structural elements of ICAM-3 D1 contributing to binding are the CD loop plus the C and F strands. In the ICAM-3/α_L I domain structure, the I domain has the metal ion coordination characteristic of the open conformation (16). Glu-37, the last residue of the C strand of ICAM-3, completes the coordination of the metal ion Mg^{2+} on the MIDAS (Fig. 1*A*), as does the counterpart Glu-34 in the ICAM-1/α_L I domain structure (16). Fig. 2*A* is a superposition of the ICAM-1/α_L I domain structure onto the ICAM-3/α_L I domain structure, with D2 of ICAM-1 omitted for clarity. The superposition was only based on framework residues of the D1s of the two ICAMs, but it is clear that as a result, the two bound I domains also overlay very well. These results show that, topologically, ICAM-3 D1 and ICAM-1 D1 dock onto the α_L I domain identically. The high-affinity mutant (K287C/K294C) α_L I domain was crystallized in the ICAM-3/α_L I domain structure, whereas the intermediate-affinity mutant (L161C/F299C) α_L I domain was used in the ICAM-1/α_L I domain structure (16). However, both complexes have similar buried surface area of about 1,250 Å^2 and the same high shape complementarity, S_c, value (24) of 0.73. This is because the intermediate-affinity I domain adopts the open conformation of the ligand-binding site when bound to ICAM-1 (16). Compared with pseudoliganded or unliganded, high-affinity α_L I domain structures (16), the high-affinity α_L I domain has the same open conformation when bound to ICAM-3 (Fig. 2*B*). The only difference is that the β5–α6 loop moves significantly toward ICAM-3 D1 after ligation and forms hydrogen bonds to the CD loop of ICAM-3 as described below. In the ICAM-1/α_L I domain structure, the same inward movement of the β5–α6 loop occurs compared with the unliganded structure (16). Conformational movement also occurs in this region upon inside-out activation of $\alpha_L\beta_2$, independent of ligand binding, as indicated by the conformation-sensitive mAb HI111, which is specific for residue Lys-268 (25). Fig. 2*A* also shows the superposition of ICAM-2 D1 onto ICAM-3 D1. A remarkable observation here is that the backbone structures of these ICAMs are most similar to one another near the $\alpha_L\beta_2$-binding interface, in particular the CD loop region.

Structure of ICAM-3 Domain 1. D1 of ICAM-3 is stable independently of D2 (26). Like ICAM-1 and -2, ICAM-3 D1 belongs to the I1 subset of the IgSF domain (13) (Fig. 1*A*). The D1s of ICAM-1 and -3 differ mainly in the BC, DE, and FG loops on the N-terminal end of the domain, which are flexible and bind to rhinovirus in ICAM-1 (27–29). The most marked structural

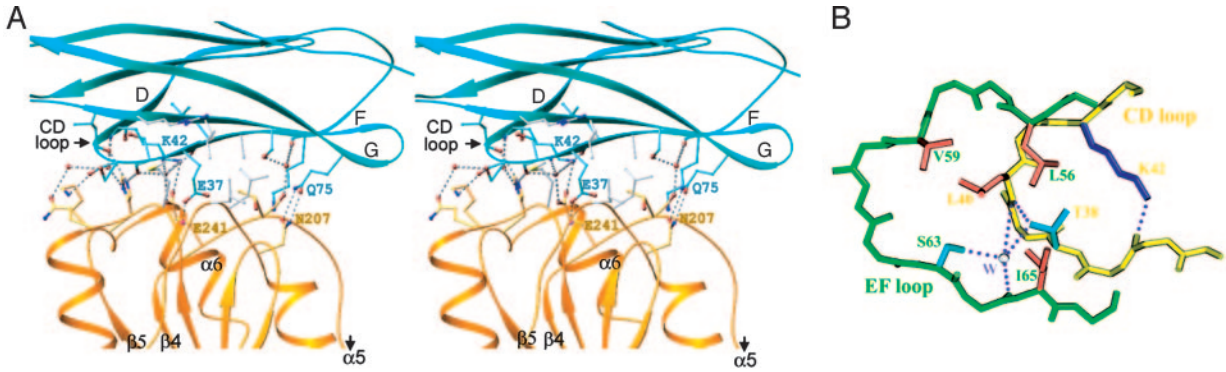

Fig. 3. The ICAM-3/$\alpha_L\beta_2$ binding interface. (*A*) The interface residues are shown in light cyan and light gold for ICAM-3 and the I domain, respectively. The metal ion, oxygens, and nitrogens are shown as magenta, red, and blue spheres, respectively. Water molecules are shown as red spheres. Metal coordination is shown by black dashed lines. Hydrogen bonds and a salt bridge between Lys-42 in ICAM-3 and Glu-241 in the I domain are represented by silver dashed lines. Residues involved in the hydrophobic patch are colored in silver. For clarity, MIDAS residues are omitted. (*B*) Structural elements that stabilize the conformation of the CD loop of ICAM-3. The CD and EF loops are colored in yellow and green, respectively. Only relevant side chains are shown in this figure for clarity. Hydrophobic, neutral hydrophilic, and basic residues are colored in orange, cyan, and blue, respectively. The broken lines represent hydrogen bonds, whereas the silver ball is a bound water molecule. *A* was prepared with RIBBONS (43), and *B* was prepared with SETOR (44).

difference is in the DE loop (Fig. 2*A*). Among D1s of ICAM-1, -2, and -3, only one insertion/deletion is found, in the DE loop (Fig. 2*C*). In the cases of ICAM-3 and -2, the D and E strands have a hairpin structure. By contrast, for ICAM-1 D1, the insertion makes the DE loop conformation much more irregular and distinctive (Fig. 2*A*). Moreover, in ICAM-3 and -2, a glycan attaches to Asn-23 with its first sugar moiety packing against the indole ring of Trp-52 (not shown), which directs the long carbohydrate side chain of the glycans toward the N terminus of the domain. An additional glycan links to the FG loop at Asn-72 and decorates the tip of the first domain in ICAM-3 (Fig. 1*A*). Those glycans are absent in the rhinovirus receptor ICAM-1 and might prevent rhinovirus binding to other ICAM molecules. Additionally, ICAM-3 and -2 are three residues longer than ICAM-1 at the N terminus (Fig. 2*C*), a characteristic that would also interfere with the attachment of the virus (30).

ICAM-3 is the most heavily glycosylated protein in the ICAM subfamily. There are five N-linked glycosylation sites on the relatively small ligand-binding domain, D1, yet none of them is on the domain's CFG face bearing the α_L-binding site. ICAM-3 D1 was treated with Endo H_f to facilitate crystallization. In electron density maps, one residual sugar moiety at each of two sites, Asn-23 on the B strand and Asn-81 on G strand, was clearly visualized. The densities for sugars at the other three sites (Asn-55, Asn-58, and Asn-72) were visible but extremely weak. The close spacing of sites at Asn-55 and Asn-58 may inhibit glycosylation of both of these asparagines. The ladder of glycoforms in SDS/PAGE of ICAM-3 D1 before Endo H treatment, and comparison after Endo H treatment, shows predominant usage of three or four of the five potential N-linked glycan sites (Fig. 1*B*). Electron densities suggest that the sites at Asn-55, Asn-58, and Asn-72 are N-glycosylated in differing subsets of ICAM-3 D1 molecules. One sugar residue each has been modeled and shown in Fig. 1*A* for illustration.

An ICAM-3/α_L Docking Mode That Is Common for ICAM Subfamily Binding to $\alpha_L\beta_2$ Integrin. At the center of the recognition site, the invariant Glu-37 of ICAM-3 coordinates to the MIDAS of the α_L I domain, surrounded by an extensive hydrogen bond network that establishes the docking specificity. One important advance from the high-resolution ICAM-3/α_L I domain structure is the visualization of four hydrogen bonds donated by I domain $\beta5$–$\alpha6$ loop side chains to the main chain carbonyl oxygens in the CD loop of ICAM-3 (Fig. 3*A*). These bonds include the bidentate hydrogen bonds from the I domain's His-264 to the carbonyl oxygens of Thr-38 and Leu-40 in ICAM-3, a hydrogen bond connection between the same His-264 and the carbonyl oxygen of Lys-42 of ICAM-3 through a water molecule, and a hydrogen bond from the I domain's Lys-263 to the carbonyl oxygen of Ser-39 (Fig. 3*A*). Because the conformation of the CD loop appears highly conserved among ICAM-1, -2, and -3 (Fig. 2*A*), the same side-chain–backbone hydrogen bonds are likely to occur in complexes with ICAM-1 and -2. A consensus L/I-E-T-S/P-L sequence in this CD loop in ICAMs has been recognized for some time (Fig. 2*C*) and, together with its counterpart sequence in VCAM, has been proposed to be a general integrin recognition motif (31, 32). Mutagenesis of CD loop residues in ICAM-3 and their counterparts in ICAM-1 and -2 greatly decreases or even abolishes binding to $\alpha_L\beta_2$ (26, 27, 33–35). Our high-resolution structure shows unambiguously that within this motif an integrated water molecule links the hydroxyl group of Thr-38 and the amide group of Leu-40 on the CD loop to the carbonyl group of Arg-64 and the hydroxyl group of Ser-63 on the F strand (Fig. 3*B*). Together with the hydrogen bond between the hydroxyl group of Thr-38 and the amide group of Leu-40, which were also seen in ICAM-1 and -2 structures (36, 37), this water helps to determine the CD loop conformation. Furthermore, the conserved Lys-42 side chain hydrogen bonds to the carbonyl group of Leu-36, clasping the two termini of the CD loop (Fig. 3*B*). On the other hand, Leu-40 has its branched side chain snuggling into a hydrophobic pocket composed of Leu-56, Val-59, and Ile-65 (Fig. 3*B*). Clearly, the invariant Thr-38 and Leu-40 residues play a key role in restraining the CD loop of ICAM family members in the same conformation. We propose that the conservation of the CD backbone enables the Lys-263 and His-264 side chains in the mobile $\beta5$–$\alpha6$ loop of the I domain to form hydrogen bonds to the CD loop backbone in recognition of all these ICAMs.

The invariant Lys residue following the CD loop, Lys-42 in ICAM-3, forms an important salt bridge to Glu-241 of the I domain (Fig. 3*A*), as also reported in the ICAM-1/α_L I domain structure (16). Allostery markedly reorients Glu-241 in the open conformation of the α_L I domain, enabling the crucial salt bridge. Reorientation in the $\beta4$–$\alpha5$ loop bearing Glu-241, including a backbone flip in Gly-240, is linked to the change from a direct to a water-mediated coordination of Asp-239 with the Mg^{2+} ion in the open, high-affinity conformation of the MIDAS (16). At the opposite edge of the interface near the FG loop of ICAM-3 D1, there is another hydrogen bond network (Fig. 3*A*). The Gln-75 residue on the FG loop forms two hydrogen bonds with

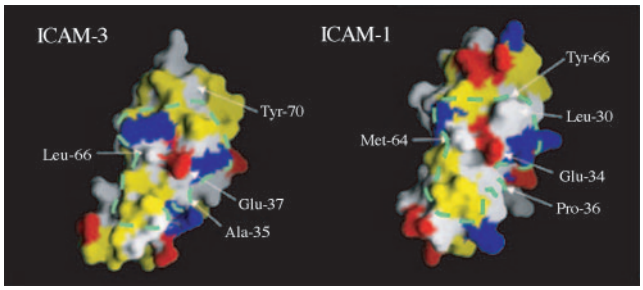

Fig. 4. Surface representation of the binding faces of ICAM-3 and -1. Negatively and positively charged residues are colored red and blue, respectively. Hydrophobic and neutral hydrophilic residues are colored white and yellow, respectively. Some important residues are labeled. The binding footprints are encircled with green dashed lines. Prepared with GRASP (45).

Asn-207 of α_L. This Gln is invariant in ICAM-1, -2, and -3 (Fig. 2*C*). Mutation of Gln-75 in ICAM-3 to His or Ala decreases or eliminates α_L binding (26, 33, 38). The corresponding residue Gln-73 in ICAM-1 and Gln-75 in ICAM-2 are also critical for binding to α_L (27, 35).

The 1.65-Å resolution ICAM-3/α_L I domain structure enables the water molecules embedded in the binding interface to be resolved. Other than those integrated within the MIDAS, there are six water molecules that become buried upon complex formation. They all connect the two binding partners through multiple hydrogen bonds. On the ICAM-3 side, mostly the backbone atoms of the C strand and CD loop are involved (Fig. 3*A*). These water molecules make the interface even more complementary.

Altogether, ICAM-3 docks to the α_L I domain through 18 specific polar interactions, directly or through water molecules, including the key MIDAS coordination at Glu-37, critical salt bridges, and hydrogen bonding networks on both sides of Glu-37. The residues engaged in these interactions, as well as the decisive CD loop conformation that establishes the docking are extremely conserved in ICAM-1, -2, and -3 (Fig. 2*C*). The conserved polar interactions suggest that most of the water molecules should also be present in other ICAM/α_L I domain complexes. The specific docking mode revealed by the ICAM-3/α_L I domain structure at a resolution of 1.65 Å and the comparison to the ICAM-1/α_L I domain (16) and ICAM-2 structures (37) reveal a common mechanism for ICAM subfamily binding to $\alpha_L\beta_2$.

Determinants of $\alpha_L\beta_2$-Binding Affinity Differences for ICAM Subfamily Members. The specific ICAM/$\alpha_L\beta_2$ recognition pattern revealed in the ICAM-3/α_L I domain structure covers a broad area of the complex interface. Given that ICAM subfamily members share the identical docking mode, an interesting question is what determines the differential binding affinity among the various subfamily members. Kinetics measurements from the association and dissociation phase in Biacore showed that the k_{on} values of ICAM-2 and -3 are similar to one another and 4- to 5-fold lower than the value of ICAM-1 (12). Furthermore, the k_{off} value of ICAM-3 is three times higher than for ICAM-1 or -2, whereas the off-rates of ICAM-1 and -2 are almost identical.

A characteristic feature of the α_L-binding surface of ICAM-3 D1 is the predominance of hydrophilic residues (Fig. 4). The only major ICAM-3 hydrophobic residue on the interface is Leu-66, which contacts Leu-204, Leu-205, and Met-140 of the I domain. Ala-35 of ICAM-3 D1 offers additional hydrophobic contacts with Thr-243 of the I domain. By comparison, significantly more hydrophobic residues can be found in the α_L-binding surface of ICAM-1 D1 (Fig. 4). Met-64 of ICAM-1 occupies the equivalent position as Leu-66 of ICAM-3. Surrounding the key MIDAS-coordinating residue Glu-34 in ICAM-1 are additional hydrophobic residues, Leu-30, Pro-36, and Tyr-66. The equivalent residues in ICAM-3 are Lys-33, Ser-39, and Ser-68. The hydrophobicity difference in the binding area between ICAM-3 and -1 is manifest. The hydrophobicity around the equivalent MIDAS-coordinating Glu residue in ICAM-2 is intermediate between ICAM-1 and -3. The hydrophobicity differences at the binding surface thus appear to explain the order of affinity of ICAM-1 > ICAM-2 > ICAM-3. Substitutions in the ICAM-1 interface that increase its hydrophobicity further enhance its affinity for the α_L I domain by decreasing k_{off} (G.S. and T.A.S., unpublished work). These findings suggest that the nonpolar environment surrounding the key MIDAS-binding Glu residue plays an important role in regulating $\alpha_L\beta_2$-binding affinity of ICAMs by mostly affecting the off-rate.

SPR measurements tested the hypothesis that the bulky car-

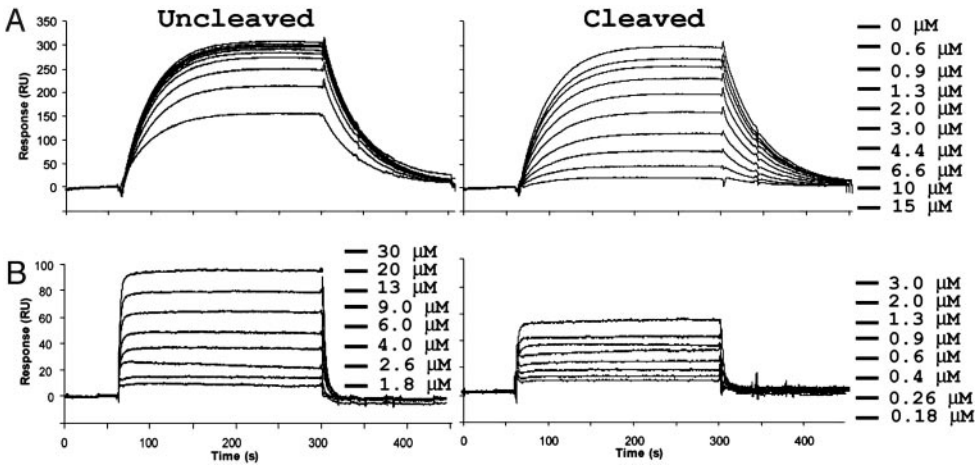

Fig. 5. Binding of the α_L I domains to ICAM-3 measured with SPR. (*A*) Inhibition assay. Endo H_f-cleaved or uncleaved ICAM-3 D1 from CHO Lec cells was mixed with high-affinity α_L I domain (50 nM) at a series of concentrations (15, 10, 6.6, 4.4, 3.0, 2.0, 1.3, 0.9, 0.6, and 0 μM) and then injected over the ICAM-1-Fc coated sensor chip at 10 μl/min in TBS/1 mM Mg^{2+}. (*B*) Direct measurement of affinity and kinetics. Sensorgrams show the binding of the uncleaved ICAM-3 D1 (30, 20, 13, 9, 6, 4, 2.6, and 1.8 μM) or Endo H_f-cleaved (3, 2, 1.3, 0.9, 0.6, 0.4, 0.26, and 0.18 μM) to I domain immobilized on streptavidin chip in TBS/1 mM Mg^{2+}. In all sensorgrams, the signals from the control surface, as described in *Methods*, were subtracted. Concentrations are shown to the right in the same order, top to bottom, as the corresponding curves.

Table 2. Effect of N-glycosylation of ICAM-3 D1 on affinity for the high-affinity α_L I domain

ICAM-3 D1	k_{on}, $M^{-1}{\cdot}s^{-1} \times 10^{-4}$	k_{off}, $s^{-1} \times 10^{2}$	K_D, μM
Uncleaved, 293T	0.88 ± 0.20	27.2 ± 5.8	25.0 ± 2.80
Uncleaved, CHO Lec	1.27 ± 0.16	26.0 ± 6.0	20.4 ± 0.80
Cleaved, CHO Lec	7.38 ± 0.77	16.2 ± 3.0	2.20 ± 0.28

The K_D value was determined from the steady-state equilibrium response levels. k_{off} was derived from curve fitting of the dissociation phase. k_{on} was calculated as k_{off}/K_D.

bohydrates attached to the glycosylation sites in ICAM-3 affect on-rate. Binding of the high-affinity α_L I domain to ICAM-3 immobilized on a SPR sensor chip was inhibited more strongly by Endo H_f-treated ICAM-3 D1 (IC_{50} = 3.0 ± 0.6 μM) than untreated ICAM-3 D1 (IC_{50} = 15 ± 1.2 μM) (Fig. 5*A*). Direct binding of three different glycoforms of ICAM-3 to immobilized high-affinity α_L I domain was also measured by SPR. ICAM-3 D1 from 293T cells (ICAM-3/293T) with complex-type carbohydrate has a slower k_{on} and similar k_{off} to ICAM-3 D1 from CHO Lec cells, which has high-mannose, Endo-H-susceptible N-linked glycans (Fig. 1*B* and Table 2). After Endo H_f treatment, the k_{on} value of ICAM-3 D1/CHO Lec binding to I domain increased 6-fold, whereas the k_{off} decreased by <2-fold (Table 2 and Fig. 5*B*). These results show that the glycans attached to D1 of ICAM-3 markedly lower its affinity for α_L primarily by lowering k_{on}. ICAM-1 D1 does not have any glycans, whereas the sites at Asn-58 and -81 in ICAM-2 and -3 and the additional site at Asn-72 of ICAM-3 encircle the binding surface. To sum up, glycans at the interface periphery differentially regulate affinity of ICAMs largely by decreasing on-rate, whereas hydrophobicity of the interface differentially regulates affinity by decreasing off-rate.

Based on the ability of mAbs to integrin $\alpha_L\beta_2$ to differentially inhibit or stimulate binding to ICAM-1, -2, and -3, it has been speculated that different conformational states of the α_L I domain (39, 40) or $\alpha_L\beta_2$ (41) differentially recognize ICAM-1 and -3. Our findings demonstrate that identical, open conformations of the α_L I domain bind to ICAM-1 and -3, and that the binding modes are indistinguishable. Therefore, other explanations for these differential effects must be sought. One possibility is that the lower affinity interaction with ICAM-3 may be more susceptible to inhibition. MEM-83 mAb to the α_L I domain, which stimulates binding to ICAM-1 and inhibits binding to ICAM-3, has been mapped to α_L I domain residues Asp-182 and Glu-21, which are distal from the ICAM-binding site (Fig. 1*A*) and do not undergo allosteric change (42). Perhaps the N-linked glycans present in D1 of ICAM-3 and not in D1 of ICAM-1, including those at ICAM-3 residues Asn-72 and -81 (Fig. 1*A*) clash with MEM-83 mAb when it is bound to the α_L I domain.

In conclusion, the 1.65-Å resolution ICAM-3/α_L I domain structure presented here suggests a common docking mode for all ICAMs that bind to $\alpha_L\beta_2$ and suggests the determinants of the differential binding affinities of ICAM-1, -2, and -3. This work provides a structural example of how a single integrin molecule $\alpha_L\beta_2$ serves as a receptor for multiple biological ligands.

We thank Rob Meijers for helpful discussion and critical reading and Michael Eck and Stephen Blacklow for reviewing the manuscript. This work was supported by National Institutes of Health Grants CA31798 and HL48675.

1. de Fougerolles, A. R., Qin, X. & Springer, T. A. (1994) *J. Exp. Med.* **179,** 619–629.
2. Butcher, E. C. (1991) *Cell* **67,** 1033–1036.
3. Springer, T. A. (1994) *Cell* **76,** 301–314.
4. Bachmann, M. F., McKall-Faienza, K., Schmits, R., Bouchard, D., Beach, J., Speiser, D. E., Mak, T. W. & Ohashi, P. S. (1997) *Immunity* **7,** 549–557.
5. de Fougerolles, A. R., Stacker, S. A., Schwarting, R. & Springer, T. A. (1991) *J. Exp. Med.* **174,** 253–267.
6. de Fougerolles, A. R. & Springer, T. A. (1992) *J. Exp. Med.* **175,** 185–190.
7. Fawcett, J., Holness, C. L., Needham, L. A., Turley, H., Gatter, K. C., Mason, D. Y. & Simmons, D. L. (1992) *Nature* **360,** 481–484.
8. Vazeux, R., Hoffman, P. A., Tomita, J. K., Dickinson, E. S., Jasman, R. L., St. John, T. & Gallatin, W. M. (1992) *Nature* **360,** 485–488.
9. Campanero, M. R., del Pozo, M. A., Arroyo, A. G., Sanchez-Mateos, P., Hernandez-Caselles, T., Craig, A., Pulido, R. & Sanchez-Madrid, F. (1993) *J. Cell Biol.* **123,** 1007–1016.
10. Montoya, M. C., Sancho, D., Bonello, G., Collette, Y., Langlet, C., He, H. T., Aparicio, P., Alcover, A., Olive, D. & Sanchez-Madrid, F. (2002) *Nat. Immunol.* **3,** 159–168.
11. Bleijs, D. A., Binnerts, M. E., van Vliet, S. J., Figdor, C. G. & van Kooyk, Y. (2000) *J. Cell Sci.* **113,** 391–400.
12. Shimaoka, M., Lu, C., Palframan, R. T., von Andrian, U. H., McCormack, A., Takagi, J. & Springer, T. A. (2001) *Proc. Natl. Acad. Sci. USA* **98,** 6009–6014.
13. Wang, J.-H. & Springer, T. A. (1998) *Immunol. Rev.* **163,** 197–215.
14. Springer, T. & Wang, J.-H. (2004) *Adv. Protein Chem.* **68,** 29–63.
15. Lee, J. O., Rieu, P., Arnaout, M. A. & Liddington, R. (1995) *Cell* **80,** 631–638.
16. Shimaoka, M., Xiao, T., Liu, J. H., Yang, Y., Dong, Y., Jun, C. D., McCormack, A., Zhang, R., Joachimiak, A., Takagi, J., Wang, J. H. & Springer, T. A. (2003) *Cell* **112,** 99–111.
17. Casasnovas, J. M. & Springer, T. A. (1995) *J. Biol. Chem.* **270,** 13216–13224.
18. Otwinowski, Z. & Minor, W. (1997) *Macromol. Crystallogr.* **276,** 307–326.
19. Navaza, J. (1994) *Acta Crystallogr. A* **50,** 157–163.
20. Jones, T. A., Zou, J.-Y., Cowan, S. W. & Kjeldgaard, M. (1991) *Acta Crystallogr. A* **47,** 110–119.
21. Brunger, A., Adams, P., Clore, G., DeLano, W., Gros, P., Grosse-Kunstleve, R., Jiang, J.-S., Kuszewski, J., Nilges, N., Pannu, N., *et al.* (1998) *Acta Crystallogr. D* **54,** 905–921.
22. Altman, J. D., Moss, P. A., Goulder, P. J., Barouch, D. H., McHeyzer-Williams, M. G., Bell, J. I., McMichael, A. J. & Davis, M. M. (1996) *Science* **274,** 94–96.
23. Crawford, F., Kozono, H., White, J., Marrack, P. & Kappler, J. (1998) *Immunity* **8,** 675–682.
24. Lawrence, M. C. & Colman, P. M. (1993) *J. Mol. Biol.* **234,** 946–950.
25. Ma, Q., Shimaoka, M., Lu, C., Jing, H., Carman, C. V. & Springer, T. A. (2002) *J. Biol. Chem.* **277,** 10638–10641.
26. Klickstein, L. B., York, M. R., Fougerolles, A. R. & Springer, T. A. (1996) *J. Biol. Chem.* **271,** 23920–23927.
27. Staunton, D. E., Dustin, M. L., Erickson, H. P. & Springer, T. A. (1990) *Cell* **61,** 243–254.
28. McClelland, A., deBear, J., Yost, S. C., Meyer, A. M., Marlor, C. W. & Greve, J. M. (1991) *Proc. Natl. Acad. Sci. USA* **88,** 7993–7997.
29. Register, R. B., Uncapher, C. R., Naylor, A. M., Lineberger, D. W. & Colonno, R. J. (1991) *J. Virol.* **65,** 6589–6596.
30. Martin, S., Martin, A., Staunton, D. E. & Springer, T. A. (1993) *Antimicrob. Agents Chemother.* **37,** 1278–1284.
31. Vonderheide, R. H., Tedder, T. F., Springer, T. A. & Staunton, D. E. (1994) *J. Cell Biol.* **125,** 215–222.
32. Osborn, L., Vassallo, C., Browning, B. G., Tizard, R., Haskard, D. O., Benjamin, C. D., Dougas, I. & Kirchhausen, T. (1994) *J. Cell Biol.* **124,** 601–608.
33. Holness, C. L., Bates, P. A., Little, A. J., Buckley, C. D., McDowall, A., Bossy, D., Hogg, N. & Simmons, D. L. (1995) *J. Biol. Chem.* **270,** 877–884.
34. Bell, E. D., May, A. P. & Simmons, D. L. (1998) *J. Immunol.* **161,** 1363–1370.
35. Casasnovas, J. M., Pieroni, C. & Springer, T. A. (1999) *Proc. Natl. Acad. Sci. USA* **96,** 3017–3022.
36. Casasnovas, J. M., Stehle, T., Liu, J.-H., Wang, J.-H. & Springer, T. A. (1998) *Proc. Natl. Acad. Sci. USA* **95,** 4134–4139.
37. Casasnovas, J. M., Springer, T. A., Liu, J. H., Harrison, S. C. & Wang, J.-h. (1997) *Nature* **387,** 312–315.
38. Sadhu, C., Lipsky, B., Erickson, H. P., Hayflick, J., Dick, K. O., Gallatin, W. M. & Staunton, D. E. (1994) *Cell Adhes. Commun.* **2,** 429–440.
39. Binnerts, M. E., van Kooyk, Y., Simmons, D. L. & Figdor, C. G. (1994) *Eur. J. Immunol.* **24,** 2155–2160.
40. Landis, R. C., McDowall, A., Holness, C. L., Littler, A. J., Simmons, D. L. & Hogg, N. (1994) *J. Cell Biol.* **126,** 529–537.
41. Ortlepp, S., Stephens, P. E., Hogg, N., Figdor, C. G. & Robinson, M. K. (1995) *Eur. J. Immunol.* **25,** 637–643.
42. Lu, C., Shimaoka, M., Salas, A. & Springer, T. A. (2004) *J. Immunol.* **173,** 3972–3978.
43. Carson, M. (1995) *Methods Enzymol.* **277,** 493–505.
44. Evans, S. V. (1993) *J. Mol. Graphics* **11,** 134–138.
45. Nicholls, A., Sharp, K. A. & Honig, B. (1991) *Proteins* **11,** 281–296.